Multiaperture Focusing for Spaceborne Transmitter/Ground-Based Receiver Bistatic SAR

Filip Rosu, Andrei Anghel, *Member, IEEE*, Remus Cacoveanu, Björn Rommen, and Mihai Datcu, *Fellow, IEEE*

***Abstract*—The article proposes a methodology to perform azimuth focusing of spaceborne transmitter-stationary receiver bistatic synthetic aperture radar data across multiple along-track apertures to increase azimuth resolution. The procedure uses as input several azimuth apertures (continuous groups of range compressed pulses) from one or more satellite bursts and comprises the following stages: antenna pattern compensation, slow time resampling, reconstruction of missing azimuth samples between neighboring sets of pulses using an autoregressive (AR) model and back-projection focusing of the resulting multiaperture range image. A novel, highly efficient method is proposed to estimate the optimal order for the AR model. It differs from the traditional approach that uses the Akaike Information Criterion to directly estimate the order because the proposed method estimates the order indirectly by detecting the number of targets using principle component analysis. Spatial smoothing is used to obtain a full rank covariance matrix, whose eigenvalues are then analyzed using minimum description length. The optimal order is an integer multiple of the number of targets, which depends on signal-to-noise ratio. The approach is evaluated with real bistatic data acquired over an area of Bucharest city, Romania.**

***Index Terms*—Autoregressive (AR) model, bistatic synthetic aperture radar (SAR), focusing, order estimation, signal reconstruction.**

I. Introduction

BISTATIC and multistatic synthetic aperture radar (SAR) systems have seen a continuous growth in popularity over the years due to their unique and powerful remote sensing capabilities. In this article, we will focus on how cross-range resolution may be improved using a bistatic SAR system composed from an opportunistic spaceborne radar sensor and a ground-based receiver.

Manuscript received March 12, 2020; revised August 12, 2020; accepted September 5, 2020. Date of publication September 18, 2020; date of current version October 5, 2020. This work was supported by the European Space Agency (ESA) through the TomoSAR-1B Project, (Single-pass Bistatic SAR Tomography), under contract 4000124573/18/NL/CBi. *(Corresponding author: Filip Rosu.)*

Filip Rosu and Andrei Anghel are with the Research Centre of Spatial Information, CEOSpaceTech, University Politehnica Bucharest, 061071 Bucuresti, Romania. (e-mail: frosu@radio.pub.ro; andrei.anghel@munde.pub.ro).

Remus Cacoveanu is with EOS Electronic Systems, 014455 Bucharest, Romania (e-mail: r_cacoveanu@yahoo.com).

Björn Rommen is with European Space Agency (ESA-ESTEC), 2201 AZ Noordwijk, The Netherlands (e-mail: bjorn.rommen@esa.int).

Mihai Datcu is with Remote Sensing Technology Institute, German Aerospace Center (DLR), 82234 Wessling, Germany, and also with the Research Centre of Spatial Information, CEOSpaceTech, University Politehnica Bucharest, 061071 Bucharest, Romania. (e-mail: mihai.datcu@dlr.de).

Digital Object Identifier 10.1109/JSTARS.2020.3025058

A certain ground location can be usually imaged with a monostatic spaceborne SAR sensor, by exploiting the information available from one ascending/descending orbit. Moreover, if the operating mode of the satellite uses multiple subswaths, this information is obtained only from one subswath per orbit.

Bistatic SAR imaging systems with a stationary receiver and a spaceborne transmitter of opportunity (e.g., TerraSAR-X [1], ERS-2/ENVISAT [2], or GNSS [3]) open the possibility to image the same area using data bursts belonging to multiple subswaths [4], [5].

When Sentinel-1A/B operating in the terrain observation through progressive scans (TOPSAR) imaging mode is used as transmitter of opportunity, a stationary receiver captures pulses from the burst corresponding to the subswath in which the receiver is placed, and also from bursts belonging to the other subswaths. In both cases, the received pulses can be pulses that were transmitted through the main beam or through the side lobes of the satellite's antenna. The available multiburst data can be used in various ways for target characterization by exploiting the enhanced azimuth diversity. A procedure to enhance the azimuth resolution using pulses received by the antenna's side lobes was presented in [4] for a bistatic receiver that records data continuously.

The principle benefit of using multiple apertures in spaceborne transmitter/stationary receiver bistatic SAR is obtaining fine azimuth resolution, having access just to publicly available information regarding the data (e.g., the Sentinel 1A/B TOPSAR ancillary information required to synchronize the bistatic system and to perform azimuth focusing). Moreover, Sentinel 1A/B does not generally operate in spotlight mode and cannot provide very good azimuth resolution. Thus, such a bistatic system can be used for fine resolution SAR imaging even when the satellite operates in TOPSAR mode and by only using publicly available information.

This article presents a methodology developed to increase azimuth resolution by exploiting multiaperture bistatic data acquired in a spaceborne transmitter–stationary receiver configuration. The procedure uses as input several continuous groups of range compressed pulses (from one or more bursts) and consists in the following main steps: compensation of the antenna pattern (AP), resampling in the slow time domain, and reconstruction of the missing azimuth samples between neighboring groups of pulses using an autoregressive (AR) model. The obtained multiaperture range image is focused on a 2-D grid with a back-projection algorithm adapted to bistatic geometry.

Compared to the method presented in [4], the procedure proposed in this article aims to exploit data from multiple bursts and is designed for a trigger-based acquisition, which reduces the memory requirements and enhances the maximum number of pulses that can be recorded. This implies an increased total aperture length (and better azimuth resolution), but the pulses that do not reach the triggering threshold will not be recorded and their information has to be extrapolated from available data. It is important to note that if a pulse is detected on the synchronization channel (line of sight), it is not necessary that reflections from all targets are also received, as some shapes might have pulse-to-pulse variations in radar cross-section, and can even migrate through range bins. However, for the analysis presented in this article, we assume that these effects are negligible.

Another important factor which is addressed in this article is the effect the order of the AR model has on the data reconstruction step. As it will be shown later in this article, setting the order too low will cause the AR model to underfit the data while setting the order too high will cause overfitting. Either case will have a negative impact on signal reconstruction. The Akaike Information Criterion (AIC), developed by Akaike, is widely used for obtaining a good balance between performance and risk of overfitting. However, the method can be extremely costly, especially for large data samples. We propose a new approach for estimating the order, based on phased array Direction of Arrival techniques, which is significantly more efficient, without compromise in performance. The traditional approach using AIC to directly estimate the optimal order will be used throughout this article as a reference for our proposed method.

The rest of this article is structured as follows. Section II presents the developed procedure to focus multiaperture bistatic data. Section III presents an in-depth analysis of the order-estimating method, while in Section IV, the methodology is evaluated with real data acquired with the receiver presented in [5]. The conclusion is then stated in Section V.

II. Multiaperture Focusing of Bistatic Data

A. Bistatic Azimuth Signal Model

The envisaged bistatic geometry is shown schematically in Fig. 1. The ground receiver has two channels—one that receives directly the transmitted pulses through an antenna oriented toward the satellite (reference channel) and another that receives the reflected signals from the illuminated scene (typically called imaging channel). The duration of each aperture k that illuminates the scene is denoted with T_k and its central azimuth time with $t_{ap,k}$, defined as the moment when the satellite reaches the center of aperture k.

The closest approach distance to the receiver and to an arbitrary point P from the scene are denoted R_0, and respectively, $R_{0,P}$.

The origin of the slow time axis corresponds to the closest point of approach to the receiver and t_P is the zero-Doppler time of point P.

At the ground receiver level, the range compression of each pulse is performed by intercorrelating the baseband signal of the imaging channel with the one of the reference channel [5], and

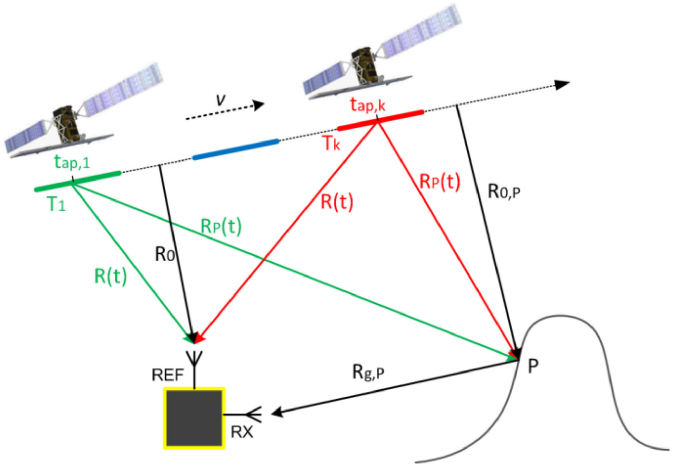

Fig. 1. Spaceborne transmitter–stationary receiver bistatic geometry.

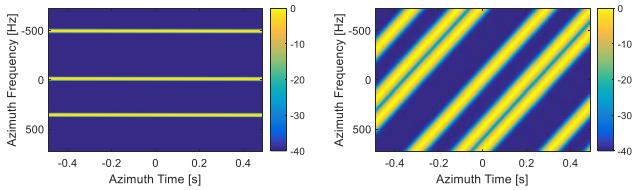

Fig. 2. Spectrogram of the azimuth chirps. (a) 3 Hz/s for the present bistatic geometry. (b) 2400 Hz/s for monostatic.

the azimuth bistatic signal of point P seen from aperture k can be expressed as

$$s_k(t) = A\exp[-j\frac{2\pi}{\lambda}(\sqrt{{R_{(0,P)}}^2 + [v(t-t_p)]^2} + R_{g,P})] \times \exp\left(j\frac{2\pi}{\lambda}\sqrt{{R_0}^2 + (vt)^2}\right) p_k(t) \cong A\exp\left(-j\frac{2\pi}{\lambda}R_{g,P}\right) \times \exp\left(j\frac{2\pi}{\lambda}\left[(R_0 - R_{0,P}) - \frac{(vt_p)^2}{2R_{0,p}} + \frac{v^2 t_p}{R_{0,p}}t\right]\right) p_k(t) \times \exp\left(j\frac{2\pi}{\lambda}\left[\frac{1}{R_0} - \frac{1}{R_{0,p}}\right]t^2\right) \quad (1)$$

where A is the complex amplitude, λ is the wavelength at central frequency, v is the satellite's velocity, and $p_k(t)$ is a window centered around $t_{ap,k}$, which includes the effect of the AP. Note that $s_k(t)$ is a chirp signal in the slow time domain with a small chirp rate (for a target placed at $R_{g,P} = 10$ km from the ground receiver and Sentinel-1 used as transmitter of opportunity, the bistatic chirp rate is around 3 Hz/s, which is a few hundred times smaller than the monostatic one), so the bistatic azimuth signal actually consists of complex exponentials with slowly varying frequency (the intercorrelation with the reference channel signal acts almost like a dechirping in azimuth). This is illustrated in Fig. 2.

From the implementation point of view, the sampled version of the signal $s_k(t)$ is a group of $N_{p,k}$ pulses acquired with a certain pulse repetition interval (PRI).

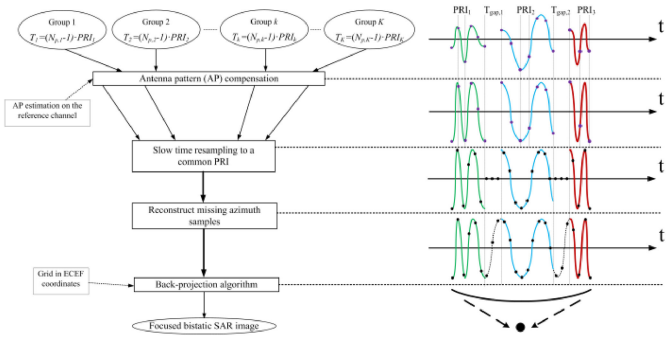

Fig. 3. Multiaperture bistatic focusing—block diagram and qualitative representation of intermediate signals.

B. Bistatic Azimuth Focusing

A block diagram of the procedure used to focus bistatic data from multiple apertures is presented in Fig. 3. We consider K groups of consecutive pulses separated by gaps having different durations. The duration of the gap between group k and $k+1$ is denoted with $T_{\text{gap},k}$. The PRI of each group depends on the burst to which it belongs (usually we have a few consecutive groups with the same PRI placed between groups with different PRIs).

Due to the beam sweep in a TOPSAR mode, each aperture (group of pulses) will be affected in a different way by the AP. Since the receive angle of the reference channel antenna is practically constant in the entire aperture, the actual AP for each group of pulses is proportional to the amplitude of the pulses received on the reference channel. Therefore, the normalized AP can be estimated on the reference channel data, and the compensation can be performed by dividing the imaging data with the AP. In [4], the AP compensation is done with a weighing window depending on the signal-to-noise ratio (SNR) in order to reduce noise amplification (however, for large SNRs, the weighing window is practically the inverse of the AP).

Since the apertures can be sampled with different PRIs, all range compressed data are resampled in slow time domain to a common PRI. If the BP focusing algorithm is applied directly on the azimuth phase history with interaperture gaps (considering as zeros the azimuth samples in between the apertures), spurious lobes will appear in the final bistatic SAR image. In a simplified manner, this effect can be thought of as a parasitic modulation, more specifically: ON-OFF keying. The ON-OFF (subaperture or gap) is the modulating signal and the azimuth chirp is the carrier. Considering the small slope of the chirp, we may approximate the signal as a complex sine-wave, so the azimuth matched filtering step simplifies to taking the Fourier Transform. Instead of a point spread function (PSF) that depends solely only on the chirp signal, we obtain the convolution between the desired PSF and the spectrum of the ON–OFF modulating signal, which produces a significant amount of sidelobes, as seen in the experimental section, Fig. 10 (b).

To avoid this effect, the next step is to fill the gaps between the apertures using an AR model [6]. An analysis was done in [7] describing the negative effects of these gaps.

Restoration of lost samples using AR models is typically used for speech and music signals, and the technique is capable to reconstruct the signal in gaps of up to 100 ms [6], [8]. This method can be used to fill the interaperture gaps of bistatic azimuth signals since they actually consist in a couple of linear chirp signals with small frequency variations (quite similar with some audio signals) that can easily be regarded as short-term stationary signals around the gaps.

In our implementation, the samples of a gap are determined as an average of the signals predicted by two AR models: one estimated using the samples from the left-side of the gap (forward prediction) and another based on the samples from the right side of the gap (backward prediction). This approach lessens the short-term stationarity requirements imposed to the signal [6]. A detailed description on how the order of the AR model is estimated will be presented next.

III. Proposed Order-Estimating Method

The proposed method, shown in Algorithm 1, can be thought of as a sequence of processing blocks, and for simplicity it will be presented as such. Subsection A presents the working principle of the order estimating method. Subsection B describes the spatial smoothing (SS) technique used to bring the sample covariance matrix, of a single acquisition, to full rank, such that the eigendecomposition required by future steps may be used for principle component analysis (PCA). Subsection C presents the minimum description length (MDL) principle used for estimating the number of detections, while in Subsection D the numerical complexity is compared to the traditional approach. Finally, Subsection E presents simulated results for the proposed subaperture stitching technique.

A. Working Principle

The proposed method uses MDL to estimate the number of spectral components, N_c, and assumes that the signal fits an AR process that has an order proportional to N_c. Similarly to Prony's method [9]–[11], the proposed method makes the assumption that the signal of interest is a series of exponentials. In theory, such a signal is described by an autoregressive moving average (ARMA) model having, in general, N_c zeros and N_c poles. However, because ARMA model estimation is computationally exhaustive, most applications approximate the model to be AR.

It is shown by Kay and Marple in [12] that, if noise is present, the N_c order AR model is very unlikely to fit the data correctly. Moreover, if the signal is a harmonic time series, the spectral estimation is highly dependent on the initial phase and in some cases, this might even lead to spectral line splitting.

In [12], the authors also present how to overcome these issues: If the number of available samples is large compared to the number of spectral components, the initial phase will have reduced impact on spectral estimation, which is further minimized by using forward–backward (FB) estimation. It is also proposed that the desired ARMA model be replaced with an AR model having a large number of poles, because an ARMA(N_c, N_c) process is equivalent to an AR(∞) process, as guaranteed by the Wold decomposition.

Algorithm 1: Processing Chain of the Proposed Method.

Input: $\boldsymbol{x}$, SNR
Output: $\boldsymbol{y}$
Choose K, α_{SNR} based on system requirements
$\hat{\boldsymbol{R}}_s = FB\ Spatial\ Smoothing(\boldsymbol{x}, K)$
$\boldsymbol{\lambda} = EigenDecomposition\ (\hat{\boldsymbol{R}}_s)$
$\hat{N}_c = MDL(\boldsymbol{\lambda}, S)$
$\dim(\hat{\boldsymbol{\theta}}) = \alpha_{\text{SNR}} \hat{N}_c$
$\boldsymbol{y} = AR(\boldsymbol{x}, \dim(\hat{\boldsymbol{\theta}}))$

Because of this, we will introduce a new SNR-dependent integer scaling variable, α_{SNR}, used to model the optimal number of parameters, $\dim(\hat{\boldsymbol{\theta}})$:

$$\dim\left(\hat{\boldsymbol{\theta}}\right) = \alpha_{\text{SNR}} \hat{N}_c. \tag{2}$$

where $\text{AR}(\boldsymbol{x}, \dim(\hat{\boldsymbol{\theta}}))$ represents the FB Burg's method [13], [14] which is used to fill the gaps of the sparse isorange data samples, $\boldsymbol{x}$, using an AR model having order $\dim(\hat{\boldsymbol{\theta}})$.

B. Forward–Backward Spatial Smoothing

Let the received signal, e.g., an arbitrary isorange, be $\boldsymbol{x} = [x(1),\ x(2),\ \ldots x(N)]^T$, with covariance matrix $\boldsymbol{R} = \boldsymbol{x}\boldsymbol{x}^H$. If only a single observation is available, $\boldsymbol{R}$ will have unitary rank, which would result in an eigendecomposition with a single nonzero eigenvalue. A possible solution to the rank deficiency problem is to use an overdetermined least squares estimate based on $P \geq N$ observations. The LS estimate is defined as $\boldsymbol{R}_{\mathbf{LS}} = \boldsymbol{X}\boldsymbol{X}^{\boldsymbol{H}}$, where $\boldsymbol{X} = [\boldsymbol{x}_1, \boldsymbol{x}_2, \ldots \boldsymbol{x}_P]$**.** However, in applications such as radar, all of the acquisitions are coherent, and thus it is impossible to increase the rank of $\boldsymbol{R}$ this way, no matter the number of observations. A popular technique used in SAR imaging for solving this problem is called range multilooking [15]. It divides the total bandwidth of the radar signal into P sub-bands and considers each a separate, noncoherent observation. The cost of using multilooking is loss in range resolution, which is greatly undesired.

In this article, we take a different approach that is frequently used in angle estimation problems, called SS. SS is used to produce full rank covariance matrices even from a single observation [16]. SS takes $\boldsymbol{x}$ and generates $N - K + 1$ smaller noncoherent signals, each having K samples, where $K \leq N/2$. The signals are of the form

$\boldsymbol{x}_{n:n+K-1} = [x(n), \ldots x(n+K-1)]^T$, with
$n = 1 : N - K + 1$. For each $\boldsymbol{x}_{n:n+K-1}$ subsignal, a K by K covariance matrix is generated as shown in Fig. 4. If $\boldsymbol{x}$ is parsed starting from 1 to $S = N - K + 1$, the method is called forward SS.

Once all $\boldsymbol{R}_{F,i}$ matrices are known, the full rank forward spatially smoothed matrix is given by (3)

$$\boldsymbol{R}_F = \sum_{i=1}^{N-K+1} \boldsymbol{R}_{F,i}. \tag{3}$$

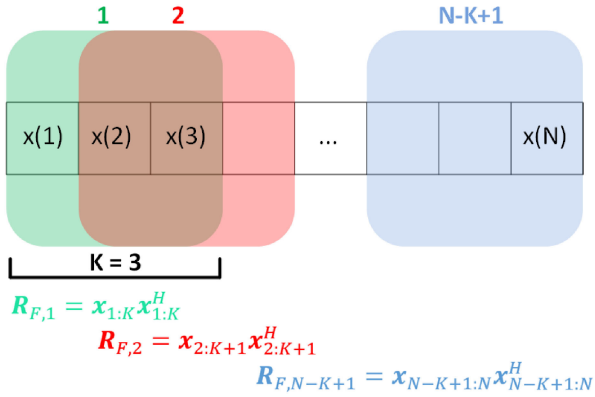

Fig. 4. Spatial smoothing for an arbitrary isorange.

Algorithm 2: Forward–Backward Spatial Smoothing.

Input: $\boldsymbol{x}, K$
Output: $\boldsymbol{R}_S$
$N = \dim(\boldsymbol{x})$
for $n = 1, \ldots N - K + 1$ **do**

$$\boldsymbol{R}_{F,n} = \begin{bmatrix} x_n^* x_n & \cdots & x_n^* x_{K+n-1} \\ \vdots & \ddots & \vdots \\ x_{K+n-1}^* x_n & \cdots & x_{K+n-1}^* x_{K+n-1} \end{bmatrix}$$

$$\boldsymbol{R}_{B,n} = \begin{bmatrix} x_{N-n+1}^* x_{N-n+1} & \cdots & x_{N-n+1}^* x_{N-n+2-K} \\ \vdots & \ddots & \vdots \\ x_{N-n+2-K}^* x_{N-n+1} & \cdots & x_{N-n+2-K}^* x_{N-n+2-K} \end{bmatrix}$$

end for

$$\boldsymbol{R}_F = \sum_{i=1}^{N-K+1} \boldsymbol{R}_{F,i}$$

$$\boldsymbol{R}_B = \sum_{i=1}^{N-K+1} \boldsymbol{R}_{B,i}$$

$$\boldsymbol{R}_S = \tfrac{1}{2}(\boldsymbol{R}_F + \boldsymbol{R}_B)$$

Backward smoothing implies parsing $\boldsymbol{x}$ from $N - K + 1$ to 1, and gives a new full-rank covariance matrix [9], $\boldsymbol{R}_B$

$$\boldsymbol{R}_B = \boldsymbol{J}\boldsymbol{R}_F^{\boldsymbol{T}}\boldsymbol{J} \tag{4}$$

where $\boldsymbol{J}$ is the exchange matrix, which has 1 elements on the counter diagonal and has all other elements equal to 0. Naturally, FB–SS implies using the two previous results together

$$\boldsymbol{R}_S = \frac{1}{2}\left(\boldsymbol{R}_F + \boldsymbol{R}_B\right). \tag{5}$$

Doing so further enhances the performance of the principal component estimators that will be used later on. The implementation of FB–SS is shown in *Algorithm 2*, where $\boldsymbol{x}$ is the input signal, with $\dim(\boldsymbol{x})$ samples, and K is the desired size of $\boldsymbol{R}_S$. The constraint to obtain full rank is that $K \leq N/2$. If $N/2$ is much larger than number of relevant eigenvalues, lowering K will greatly decrease numerical complexity when computing the eigenvalues of $\boldsymbol{R}_S$.

C. Minimum Description Length

Information criteria are widely used in parameter estimation problems [17]. The first of its kind was introduced by Akaike [18], as the "A Information Criterion". AIC makes use of the Kullback–Leibler information, $D(\boldsymbol{\theta}, \sigma^2)$, as a measure of discrepancy between the operating and approximating models

$$D\left(\boldsymbol{\theta}, \sigma^2\right) = E\left\{-2\log\left(L\left(\boldsymbol{X}\middle|m\left(\hat{\boldsymbol{\theta}}\right)\right)\right)\right\} \tag{6}$$

where $L(\boldsymbol{X}|m(\hat{\boldsymbol{\theta}}))$ denotes the likelihood function for the data, $\boldsymbol{X}$, under the approximating model $m(\hat{\boldsymbol{\theta}})$. Assuming a Gaussian distribution, we have

$$D\left(\theta, \sigma^2\right) = -2E \left\{\log\left(\frac{1}{\left(2\pi\sigma^2\right)^{\frac{N}{2}}}\exp\left(-\frac{\left(x-m\left(\hat{\boldsymbol{\theta}}\right)\right)^H\left(x-m\left(\hat{\boldsymbol{\theta}}\right)\right)}{2\sigma^2}\right)\right)\right\}. \tag{7}$$

In practice, $D(\theta, \sigma^2)$ is unknown, but can be estimated if certain assumptions are made. The AIC was designed as an estimate of $D(\theta, \sigma^2)$, and is given by

$$AIC\left(\hat{\boldsymbol{\theta}}\right) = -2\log\left(\sigma^2_{\dim\left(\hat{\boldsymbol{\theta}}\right)}\right) + 2\dim\left(\hat{\boldsymbol{\theta}}\right) \tag{8}$$

where $\dim(\hat{\boldsymbol{\theta}})$ is the selected order for the approximating model $m(\hat{\boldsymbol{\theta}})$, and $\sigma^2_{\dim(\hat{\boldsymbol{\theta}})}$ is a biased estimate of the true variance for the given model [19]

$$\sigma^2_{\dim\left(\hat{\boldsymbol{\theta}}\right)} = \left|x_N - \sum_{k=1}^{\dim\left(\hat{\boldsymbol{\theta}}\right)} x_{N-k}\hat{\theta}_k\right|^2. \tag{9}$$

In short, AIC can be described as a penalized likelihood that offers an optimal compromise between goodness of fit and complexity.

The traditional approach for estimating the order for an AR model is to compute all possible values of $\sigma^2_{\dim(\hat{\boldsymbol{\theta}})}$ and choose the order that minimizes (8). Because the AR model and the prediction error must be recomputed for every possible value of $\dim(\hat{\boldsymbol{\theta}})$, this approach will lead to a numerical complexity of $O(N^3)$. Since N can be quite large in the case of azimuth signal reconstruction, the method may become too computationally exhaustive to be practical.

The method proposed in this article does not only solve the complexity issue at no performance loss, but may also offer better estimates if properly calibrated. Instead of directly estimating the optimal value for $\dim(\boldsymbol{\theta})$, a different approach is taken that uses a principle similar to AIC, called MDL, to indirectly estimate $\dim(\boldsymbol{\theta})$.

MDL was derived by Rissanen [20] as a principle for statistical modeling of the description length. Description length can be thought of as the number of digits in a binary string used to code the data, and can be mathematically modeled as the sum of two terms. The first term is a measure of how well the model fits the data, while the second term represents the complexity of the model and encodes the parameters of the model itself [20]. MDL chooses the description length that minimizes relation (10)

$$\mathrm{MDL}\left(\hat{\boldsymbol{\theta}}\right) = -\log\left(L\left(\boldsymbol{X}\middle|m\left(\hat{\boldsymbol{\theta}}\right)\right)\right) + \eta\log\left(S\right) \tag{10}$$

where η is the number of independent parameters in $m(\hat{\boldsymbol{\theta}})$, and S represents the number of spatially smoothed matrices, computed in the previous section as $N - K + 1$. By comparing the information criterion in (8) and the description length in (10), it is seen that second term plays the role of penalty factor for MDL. As previously described, the slow-time signature of a reflective point in the proposed bistatic SAR geometry will result in a slow-varying chirp. For the sole purpose of estimating the number of detections, the slow-time response will be approximated as a sine-wave. Assuming that the targets are separable in space, the number of detections will coincide with the number of discrete frequency components, N_c. We have now simplified the problem, from estimating the number of target signatures to estimating the number of discrete frequency components using MDL which is described in detail in the following paragraphs.

An appropriate model for the family of covariance matrices to be considered is given by

$$\boldsymbol{R} = \boldsymbol{\psi} + \sigma^2\boldsymbol{I} \tag{11}$$

where $\boldsymbol{\psi}$ denotes a positive semi definite matrix, and σ^2 is the noise variance. (11) can be rewritten as

$$\boldsymbol{R} = \sum_{i=1}^{K}\left(\Lambda_i - \sigma^2\right)\boldsymbol{V}_i\boldsymbol{V}_i^H + \sigma^2\boldsymbol{I} \tag{12}$$

where $\Lambda_{1\ldots K}$ and $\boldsymbol{V}_{1\ldots K}$ are the eigenvalues and eigenvectors of $\boldsymbol{R}$, respectively, and K represents the dimension of the spatially smoothed covariance matrix. Since in our application the signal model, $m(\hat{\boldsymbol{\theta}})$, can be completely described by $\boldsymbol{R}$, it follows that [21]

$$m\left(\hat{\boldsymbol{\theta}}\right) = \left(\sigma^2, \boldsymbol{V}_1^H \ldots \boldsymbol{V}_K^H, \Lambda_1 \ldots \Lambda_K\right). \tag{13}$$

Considering that each observation, or spatially smoothed data vector, is statistically independent and regarded as a zero-mean complex Gaussian vector, their joint probability density is given by

$$f\left(\boldsymbol{X}\middle|m\left(\hat{\boldsymbol{\theta}}\right)\right) = \prod_{i=1}^{S}\frac{1}{\pi^K\det\left(\boldsymbol{R}\right)}\exp\left(-\boldsymbol{x}_{s,i}^H\boldsymbol{R}^{-1}\boldsymbol{x}_{s,i}\right) \tag{14}$$

where $\boldsymbol{x}_{s,i}$ represents the ith of S spatially smoothed vectors, of size K, illustrated in Fig. 4. Further on, it is shown in [21] that by taking the logarithm and omitting terms that do not depend on the model, we find that the log-likelihood function becomes

$$\log\left(L\left(\boldsymbol{X}\middle|m\left(\hat{\boldsymbol{\theta}}\right)\right)\right) = -S\log\left(\det\left(\boldsymbol{R}\right)\right) - \mathrm{tr}\left(\boldsymbol{R}^{-1}\hat{\boldsymbol{R}}_S\right) \tag{15}$$

where notations $\det(.)$ and $\mathrm{tr}(.)$ represent the determinant and trace of the matrix, respectively, $\hat{\boldsymbol{R}}_S$ is the spatially smoothed sample covariance matrix, and $\boldsymbol{R}$ represents the unique covariance matrix formed from the chosen model parameters. The maximum likelihood estimate is the $m(\hat{\boldsymbol{\theta}})$ that maximizes (15).

Algorithm 3: Minimum Description Length.

Input: $\boldsymbol{\lambda}, S$
Output: $\hat{N}_c$
$K = \dim(\boldsymbol{\lambda})$
for $n = 1, \dots K-1$ **do**
$\mathrm{MDL}(n) = -S(K-n)\log\left(\frac{\sqrt[K-n]{\prod_{i=n}^{K}\lambda_i}}{\frac{\sum_{i=n}^{K}\lambda_i}{K-n}}\right) + \frac{1}{2}(n(2K-n))\log(S)$
end for
$\hat{N}_c = \underset{n}{\arg\min}\{\mathrm{MDL}(n)\}$

These estimates are given by [21], [22]

$$\boldsymbol{\Lambda} = \boldsymbol{\lambda} \tag{16a}$$

$$\boldsymbol{V} = \boldsymbol{v} \tag{16b}$$

$$\hat{\sigma}^2 = \frac{\sum_{i=\hat{N}_c+1}^{K}\lambda_i}{K-\hat{N}_c} \tag{16c}$$

where $\boldsymbol{v}, \boldsymbol{\lambda}$ represent the eigenvectors and eigenvalues of the sample covariance matrix. A keynote is that the eigenvalues are sorted in descending order, such that the first $\hat{N}_c$ eigenvalues correspond to detections, while the last $K-\hat{N}_c$ correspond to noise. Finally, the maximum likelihood estimate of the noise variance, $\hat{\sigma}^2$, becomes the average of the noise eigenvalues. Replacing $\boldsymbol{R}$ with the maximum likelihood estimate, (16), gives

$$-\log\left(L\left(\boldsymbol{X}|\sigma^2, \boldsymbol{v}, \boldsymbol{\lambda}\right)\right) = -\log\left(\frac{\sqrt[K-\hat{N}_c]{\prod_{i=\hat{N}_c}^{K}\lambda_i}}{\frac{\sum_{i=\hat{N}_c}^{K}\lambda_i}{K-\hat{N}_c}}\right)^{(K-\hat{N}_c)S} \tag{17}$$

which is equivalent to the first term in (10). The term in brackets represents the ratio of the geometric mean to the arithmetic mean of the smallest $K-\hat{N}_c$ eigenvalues.

Unlike AIC, MDL also takes into account the number of independent observations, which is equivalent to the number of spatially smoothed matrices, S. This makes MDL tend toward lower-dimensional models which is a key property when used in the present application, as it avoids overfitting.

Further on, a simple example is presented, in which MDL is performed on a $K = 32$ sized vector, $x(n)$, composed of three spectral components, $N_c = 3$.

$$x(n) = \sum_{i=1}^{N_c=3} A_i e^{j\omega_i n} + w(n) \tag{18}$$

where A_i and ω_i represent the amplitude and angular frequency, respectively, of each spectral component, and $w(n)$ is complex additive white noise. The SNR used is 10 dB, and the amplitude dynamic used in this example is $\frac{\max\{\boldsymbol{A}\}}{\min\{\boldsymbol{A}\}} = 10^4$. Fig. 5 presents the evolution of the MDL cost function as $\dim(\hat{\boldsymbol{\theta}})$ increases. The value of $\dim(\hat{\boldsymbol{\theta}})$ at which the cost function is minimized represents the most probable value of N_c.

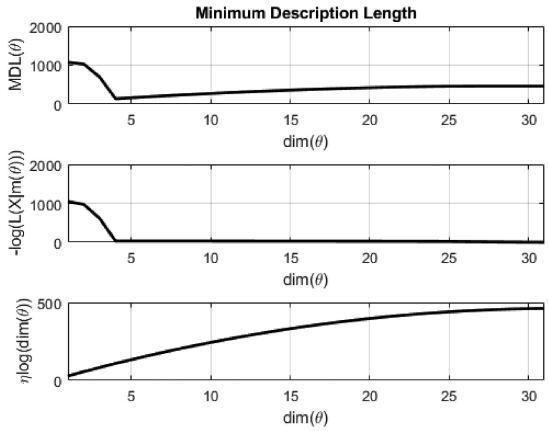

Fig. 5. $\mathrm{MDL}(\hat{\boldsymbol{\theta}})$ as a function of $\dim(\hat{\boldsymbol{\theta}})$, using the notations in relation (10).

D. Numerical Complexity

Throughout the experiments in this article, the size of the spatialy smoothed matrix, K, was empirically chosen to be $K = \frac{N}{\log_2 N}$, as it offers a good balance between efficiency and performance. In practice, K should be as small as possible, but at least twice as large as the largest possible number of targets.

The algorithms used for AR model generation have a numerical complexity of $O(N\dim(\boldsymbol{\theta}) + \dim(\boldsymbol{\theta})^2)$. By estimating the order with the classic approach, the AR algorithm must be recomputed for every possible $\dim(\boldsymbol{\theta})$ in order to evaluate the AIC described by (8). The largest theoretical value of $\dim(\boldsymbol{\theta})$ is $N-1$, thus requiring $\sum_{k=1}^{N-1} Nk + k^2$ computations, and this excludes the AIC criterion minimization and prediction error estimation. This gives a total method complexity of $O(N^3)$.

Unlike the previous method, the present method only computes the AR model once. The magnitude of the complexity is approximately $O(NK^2)$, where NK^2 is the numerical complexity of the most expensive processing block, SS. Using the proposed value for $K = \frac{N}{\log_2 N}$, the complexity gain of the method, compared to the traditional, AIC-based, method is approx. $(\log_2 N)^2$. This gain can further be increased for large *N*, depending on how sparse the image is. The raw SAR image used to provide the experimental results in this article has 10 000 range samples and 3700 cross-range samples. The reconstruction is done for each isorange, consisting in a 3700 sample vector.

The largest aperture is approximately $N = 1000$ samples. Thus, using the proposed method leads to a computational gain of 100. The traditional method's complexity could also be reduced by stopping at the first local minimum, but will no longer ensure optimal performance.

E. Numerical Results

Further on, a performance comparison is presented between the proposed method and the traditional method. Simulation parameters have been chosen to mimic the experimental bistatic SAR scenario, where the signals of interest represent the slow time response of a given number of targets. The geometry specifications were chosen to match those in our experimental setup

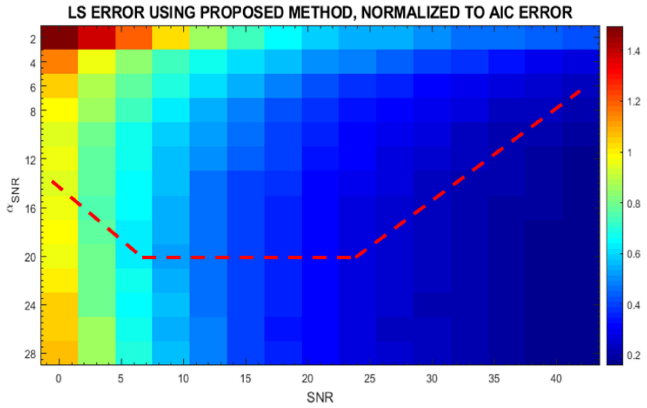

Fig. 6. RMSE of the AR model when using $\dim(\boldsymbol{\theta})$ estimated with the proposed method, as a function of SNR and parameter α_{SNR}.

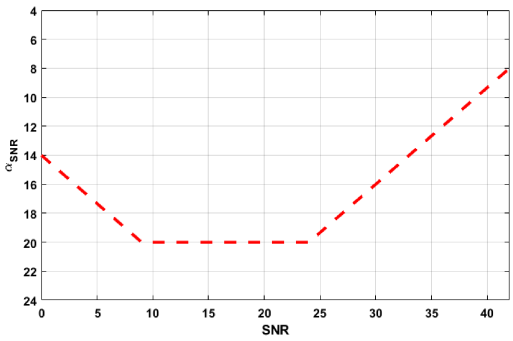

Fig. 7. Optimal values for α_{SNR}, selected from Fig. 6.

(e.g., Sentinel 1A/B height, velocity, bandwidth, and receiver sampling rate). The RMS error was computed between the ideal, artificially generated signal, and the AR-filled gaps based on the estimated $\dim(\boldsymbol{\theta})$. For both the proposed and classic order estimation methods, signal reconstruction was done with Burg's method. The RMS error was averaged over 10 000 realizations. The number of targets was set randomly between 1 and 8, and the gap size was set between 0 and 0.1 s.

Fig. 6 presents the rms error as a function of two variables; the first is α_{SNR} which is related to $\dim(\boldsymbol{\theta})$ by (2), and the second is the SNR of the input signal. A key observation is that, by choosing large values for α_{SNR}, which result in large orders when the SNR is low, the error will begin to increase. This is caused by the previously mentioned effect of overfitting.

In Fig. 7, the optimal values of α_{SNR} are shown, chosen as a compromise between performance and complexity, based on the results of Fig. 6. The SNR value was defined for the weakest point-target after azimuth compression.

Fig. 8 presents a comparison between the results of the classic method, the proposed method when α_{SNR} has a constant value of 8, and when α_{SNR} takes different values depending on the SNR, assuming it is a priori estimated. The values of α_{SNR} as a function of SNR were chosen from Fig. 6.

IV. Experimental Results

This section presents an evaluation of the proposed multiaperture focusing procedure with a bistatic acquisition performed

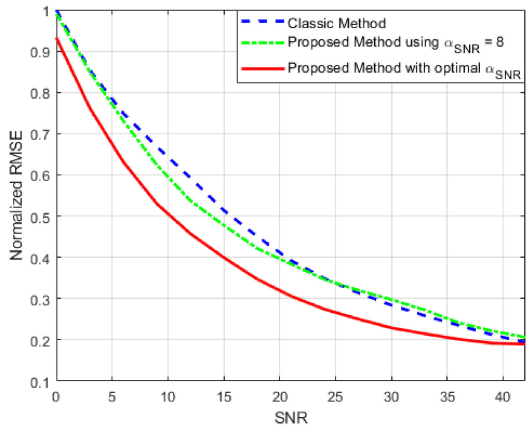

Fig. 8. Comparison between the classic method and the proposed method with $\alpha_{\mathrm{SNR}} = 8$ and with optimal α_{SNR}.

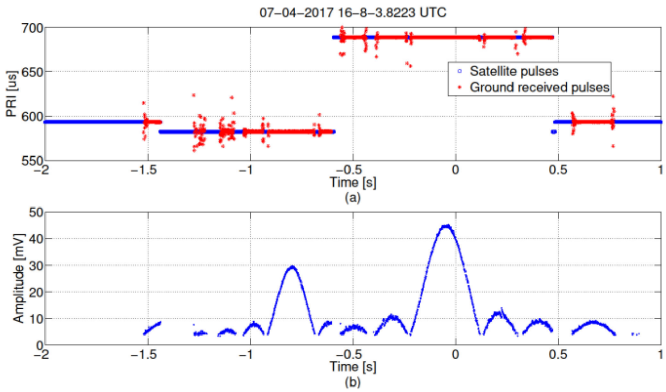

Fig. 9. Received pulses for the acquisition performed on 07.04.2017. (a) PRI (nominal and computed from the time stamps). (b) Amplitude.

on 07.04.2017 over an area of Bucharest city, Romania, with the ground receiver being placed on top of the rectorate building of University Politehnica of Bucharest and the Sentinel-1B satellite flying on an ascending orbit. The implementation details of the ground receiver are presented in [5].

The PRI and amplitude of the received pulses versus slow time are shown in Fig. 9. Fig. 9(a) displays the nominal PRI for each subswath and the PRI computed as difference between consecutive GPS timestamps stored by the ground receiver, whereas Fig. 9(b) shows the amplitude of each received pulse. The maximum amplitude is obtained for the burst from subswath 2 (with 689 μs PRI), but there are also pulses received from bursts belonging to subswaths 1 and 3.

A. Signal Reconstruction Assessment

In this subsection, we assess the impact of the AR-based signal reconstruction on the focused image. In this regard, we consider only the main beam of the azimuth signal (between -0.21 and 0.11 s slow time) and artificially introduce gaps of different sizes in the middle of the lobe. The multiaperture focusing procedure is applied on the resulting signal (two apertures with one continuous gap in between) with and without the signal reconstruction stage. The focused bistatic images are compared with the reference one obtained without any gap (classical

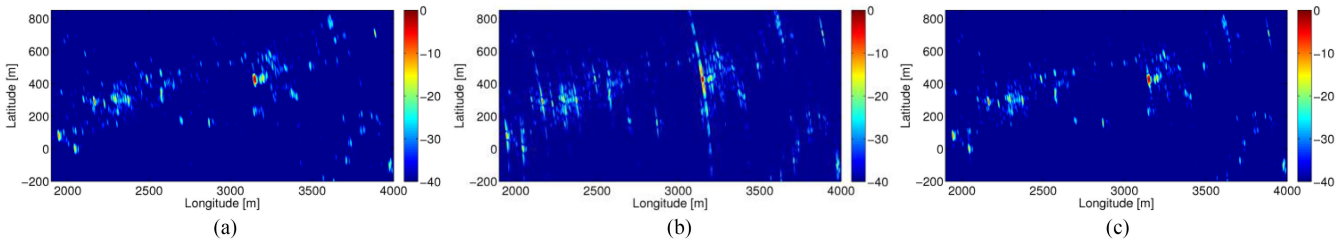

Fig. 10. Azimuth signal reconstruction assessment in multiaperture focusing for an artificially introduced gap of 50 ms. (a) Reference image. (b) Focused image with the gap filled with zeros. (c) Focused image with AR model-based filled gap.

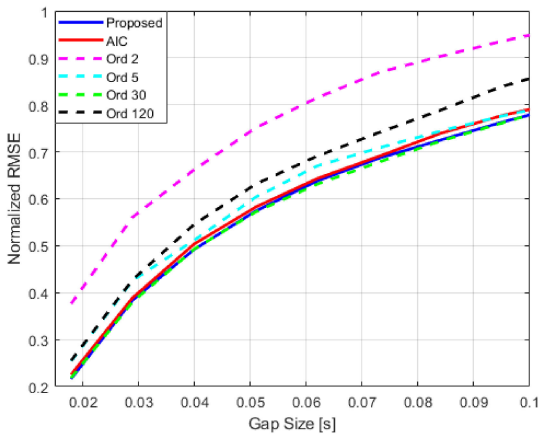

Fig. 11. RMS Error of the AR model when using different order estimating methods, normalized to the largest error.

focusing). The grid used in the BP algorithm is aligned with the latitude/longitude axis and its origin is the receiver's position.

Fig. 10(a) presents the reference image, Fig. 10(b) displays the focused image with zero-filled gaps, while Fig. 10(c) shows the focused image after AR model-based gap filling for a 50 ms gap duration. The negative impact of the zero-filled focusing is clear, and thus the method is of little practical interest. In Fig. 11, we present the root mean squared error (RMSE) of the reconstructed signals, for the two order-estimating methods and for various constant orders, as a function of gap size. The RMSE is computed between the complex reconstructed samples and the original samples. The parameters of the proposed order-estimating method were $K = \frac{N}{\log_2 N}$, and $\alpha_{\mathrm{SNR}} = 8$.

The results clearly illustrate that if the order is chosen either too high or too low, the signal will not be correctly reconstructed due to overfitting or underfitting, respectively. The reconstruction was done for an isolated, highly reflective target, situated at relative coordinates (457,3152).

Table I presents the corresponding phase errors of the isolated peak, after azimuth compression. The true phase is 93.45°.

In Table II, instead of reconstructing a strong isolated target as before, the reconstruction is done for a cluster positioned at coordinates (306,2296) relative to the receiver. The true phase of the target of interest is 146.16°. The RMSE is presented in Fig. 12.

The parameters for the proposed methods are kept the same as in the previous experiment. It is shown that by choosing

TABLE I
PHASE ERROR FOR AN ISOLATED TARGET

AR Order	Phase [deg]	Error [deg]
Proposed Method	93.338	0.112
AIC Method	93.6	0.15
2	93.042	0.408
5	93.19	0.26
30	93.371	0.079
120	93.72	0.27

TABLE II
PHASE ERROR FOR CLUSTERED TARGETS

AR Order	Phase [deg]	Error [deg]
Proposed Method	145.72	0.44
AIC Method	145.5	0.66
2	143.97	2.19
5	144.73	1.43
30	145.14	1.02
120	145.7	0.46

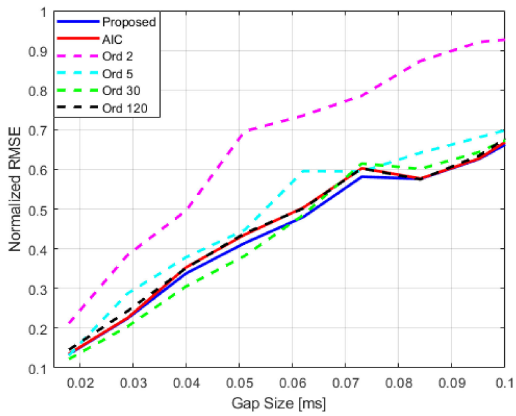

Fig. 12. RMS error of the AR model when using different order estimating methods, normalized to the largest error, for an area with many reflectors.

a constant order the error becomes highly unpredictable, and both underfitting and overfitting become an issue. An interesting result is that for a similar RMS error, overfitting has less impact on phase reconstruction than underfitting.

B. Resolution Enhancement

To emphasis the azimuth resolution enhancement that can be obtained by multiaperture focusing, we applied the procedure on

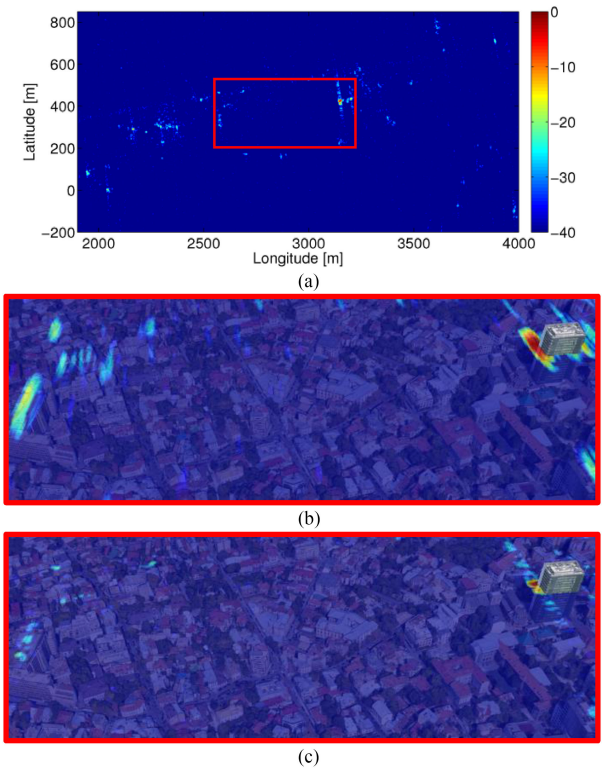

Fig. 13. Resolution enhancement with multiaperture focusing. a) is a high resolution multiaperture focused bistatic SAR image; b) and c) are focused images overlaid on Google Earth of the area inscribed by the red rectangle in a), where image b) was generated using single aperture focusing, while image c) was generated using the proposed multiaperture focusing methodology.

the azimuth signal shown in Fig. 9 for the groups of consecutive pulses between −1.02 to 0.76 s. In this interval, the maximum gap size is below 0.1 s. The resulting multiaperture bistatic SAR image [Fig. 10(a)] is focused on the same grid as the single-aperture image shown in Fig. 13(a). Fig. 13(b) and (c) present the single-aperture bistatic image and the multiaperture bistatic image of a high-rise building overlaid on a Google Earth picture, respectively.

Based on the main response of the building, the measured −6 dB resolution for the single-aperture image is 34.2 m, while for the multiaperture one is 6.8 m. Besides the drawback of a few focusing artifacts (that yield a measured peak to side lobe ratio of around 26 dB), in the multiaperture image the scattering centers are much more clearly highlighted than in the single-aperture case.

For the extended aperture, the proposed order-estimating method was approx. 30 times faster, on average, than the traditional method.

V. Conclusion

This article presented a methodology on how to focus spaceborne transmitter–stationary receiver bistatic data that span several along-track apertures with gaps in between. The possibility of increasing the azimuth resolution by using the proposed procedure was shown on a dataset acquired with Sentinel-1B operating in TOPSAR mode as transmitter of opportunity. Each subaperture is normalized with the AP and interpolated on a common grid (PRI). The gaps between the apertures are then filled using an AR model. Furthermore, a novel and highly efficient method is proposed to estimate the optimal order for the AR model. Unlike the traditional approach which uses the AIC to directly estimate the order, the proposed method indirectly estimates the order by detecting the number of targets using PCA. The optimal order is chosen as an integer multiple of the number of targets, which depends on SNR.

References

[1] F. Behner, S. Reuther, H. Nies, and O. Loffeld, "Synchronization and processing in the HITCHHIKER Bistatic SAR experiment," *IEEE J. Sel. Topics Appl. Earth Observ. Remote Sens.*, vol. 9, no. 3, pp. 1028–1035, Mar. 2016.

[2] S. Duque *et al.*, "Repeat-pass interferometry using a fixed-receiver and ERS-2/ENVISAT as transmitters of opportunity," in *Proc. IEEE Int. Geosci. Remote Sens. Symp.*, Jul. 2009, pp. II-246–II-249.

[3] X. Fan *et al.*, "Passive SAR with GNSS transmitters: Latest results and research progress," in *Proc. IEEE Int. Geosci. Remote Sens. Symp.*, Jul. 2017, pp. 1043–1046.

[4] V. Kubica, X. Neyt, and H. D. Griffiths, "Along-track resolution enhancement for bistatic SAR imaging in burst-mode operation," *IEEE Trans. Aerosp. Electron. Syst.*, vol. 52, no. 4, pp. 1568–1575, Aug. 2016.

[5] A. Anghel, R. Cacoveanu, A. Moldovan, B. Rommen, and M. Datcu, "COBIS: Opportunistic C-band bistatic SAR differential interferometry," *IEEE J Sel. Topics Appl. Earth Observ. Remote Sens.*, vol. 12, no. 10, pp. 3980–3998, Oct. 2019.

[6] W. Etter, "Restoration of a discrete-time signal segment by interpolation based on the left-sided and right-sided autoregressive parameters," *IEEE Trans. Signal Process.*, vol. 44, no. 5, pp. 1124–1135, May 1996.

[7] A. Anghel, R. Cacoveanu, B. Rommen, and M. Datcu, "Multi-aperture focusing in spaceborne transmitter-stationary receiver bistatic SAR," in *Proc. Int. Geosci. Remote Sens. Symp.*, 2019, pp. 1120–1123.

[8] I. Kauppinen and K. Roth, "Audio signal extrapolation—Theory and applications," in *Proc. 5th Int. Conf. Digit. Audio Effects*, Sep. 2002, pp. 105–110.

[9] H. Ding and B. F. Chao, "Detecting harmonic signals in a noisy time-series: The z-domain autoregressive (AR-z) spectrum," *Geophys. J. Int.*, vol. 201, no. 3, pp. 1287–1296, 2015.

[10] C. E. Froberg, *Introduction to Numerical Analysis*, 2nd ed. Reading, MA, USA: Addison-Wesley, 1969.

[11] B. F. Chao, "On the use of maximum entropy/autoregressive spectrum in harmonic analysis of time series," *Pure Appl. Geophys.*, vol. 134, pp. 303–311, 1990.

[12] S. M. Kay and S. L. Marple, "Spectrum analysis—A modern perspective," *Proc. IEEE*, vol. 69, no. 11, pp. 1380–1419, Nov. 1981.

[13] S. Marple, "A new autoregressive spectrum analysis algorithm," *IEEE Trans. Acoust., Speech, Signal Process.*, vol. 28, no. 4, pp. 441–454, Aug. 1980.

[14] J. P. Burg, "Maximum entropy spectral analysis," Ph.D. dissertation, Dept. Geophys., Stanford Univ., Stanford, CA, USA, May 1975.

[15] L. Veci, "SAR basics tutorial," Sentinel-1 Toolbox, 2015. [Online]. Available: http://step.esa.int/docs/tutorials/S1TBX%20SAR%20Basics%20Tutorial.pdf. Accessed: Feb. 27, 2020.

[16] P. Stoica and R. Moses, *Spectral Analysis of Signals*. Upper Saddle River, NJ, USA: Prentice Hall, 2005, pp. 168–170.

[17] P. Stoica and Y. Selen, "A review of information criterion rules," *IEEE Signal Process. Mag.*, vol. 21, no. 4, pp. 36–47, Jul. 2004.

[18] H. Aikaike, "Fitting autoregressive models for prediction," *Ann. Inst. Statist. Math.*, vol. 21, pp. 243–247, 1969.

[19] C. M. Hurvich and C. L. Tsai, "Regression and times series model selection in small samples," *Biometrika*, vol. 76, no. 2, pp. 297–307, 1989.

[20] A. Barron, J Rissanen, and B. Yu, "The minimum description length principle in coding and modeling," *IEEE Trans. Inf. Theory*, vol. 44, no. 6, pp. 2743–2760, Oct. 1998.

[21] M. Wax and T. Kailath, "Detection of signals by information theoretic criteria," *IEEE Trans. Acoust., Speech, Signal Process.*, vol. 33, no. 2, pp. 387–392, Apr. 1985.

[22] V. K. Madisetti and D. B. Williams, *Digital Signal Processing Handbook*. Cleveland, OH, USA: CRC Press, 1999, pp. 1426–1436.

Filip Rosu received the M.Sc. degree in communication circuits and systems from Politehnica University of Bucharest (UPB), Bucharest, Romania, in 2018. He is currently working toward the Ph.D. degree in multistatic synthetic aperture radar at the UPB.

He is currently a Radar Systems Engineer with NXP Semiconductors, Bucharest, Romania, The Netherlands. His research interests include multistatic synthetic aperture radar, mostly for earth-observation applications, signal processing, machine learning, and phased array design for the next generation of radar systems used in assisted and autonomous driving.

Andrei Anghel (Member, IEEE) received the engineering (as valedictorian) and M.S. degrees (with the highest grade) in electronic engineering and telecommunications from the University Politehnica of Bucharest, Bucharest, Romania, in 2010 and 2012, respectively, and the joint Ph.D. degree (*summa cum laude*) in signal, image, speech, and telecoms from the University of Grenoble Alpes, Grenoble, France, and in electronic engineering and telecommunications from the University Politehnica of Bucharest, Bucharest, Romania, in 2015.

Between 2012 and 2015, he was a Doctoral Researcher with Grenoble Image Speech Signal Automatics Laboratory (GIPSA-lab), Grenoble, France. In 2012, he was with the University Politehnica of Bucharest as a Teaching Assistant, where he is currently an Associate Professor with the Telecommunications Department, Faculty of Electronics, Telecommunications and Information Technology. He has authored more than 50 scientific publications, two textbooks, and a book about SAR signal processing for infrastructure monitoring. His research interests include remote sensing, radar, microwaves, and signal processing.

Dr. Anghel regularly acts as a Reviewer for several IEEE and IET journals. He was the recipient of two gold medals (in 2005 and 2006) at the International Physics Olympiads.

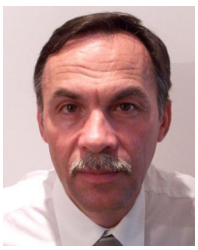

Remus Cacoveanu received the M.S. degree in electronics and telecommunications from the "Politehnica" University of Bucharest (UPB), Bucharest, Romania, in 1983, and the Ph.D. degree in microwave, optics and optoelectronics from the Institut National Politechnique de Grenoble INPG, Grenoble, France, in 1997.

He was an Associate Professor in telecommunications with UPB. For more than 10 years, he was the Technical Lead with the Redline Communications' Romanian branch, and between 2011 and 2015, he was a Technical Consultant with Blinq Networks Canada. Since 2016, he has been a Lead Scientist with EOS Electronic Systems. His research interests include wireless communication systems, antennas, radar sensors, propagation, and microwave circuits.

Björn Rommen received the M.S. degree in electrical engineering from Delft University of Technology, Delft, the Netherlands, in 1999.

From 1999 onwards, he has been working in the field of Earth observation with the Research and Technology Centre of the European Space Agency, Noordwijk, The Netherlands. He is currently a Mission Scientist with ESA's Biomass mission as well as for the Earth Explorer 10 candidate mission Harmony. His research interests include wide range within the domain of active microwave remote sensing—involving work at both microwave instrument conceptual level as well as leading R&D activities investigating wave interaction with the Earth's surface (including bio/geophysical parameter retrieval) and atmosphere—which for a large extent has been driven by SAR missions in preparation at the European Space Agency. He has been involved in the Sentinel-1A and -1B prelaunch and postlaunch activities including the commissioning phases covering overall SAR in-orbit performance and system calibration activities. His research interests include electromagnetics theory, computational electromagnetics, and radar remote sensing.

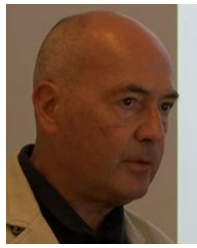

Mihai Datcu (Fellow, IEEE) received the M.S. and Ph.D. degrees in electronics and telecommunications from the University Politehnica Bucharest (UPB), Bucharest, Romania, in 1978 and 1986, respectively, and the habilitation a Diriger Des Recherches degree in computer science from the University Louis Pasteur, Strasbourg, France, in 1999.

From 1992 to 2002, he had a longer Invited Professor Assignment with the Swiss Federal Institute of Technology (ETH Zurich), Zurich, Switzerland. He was a Visiting Professor with the University of Oviedo, Oviedo, Spain; University Louis Pasteur; International Space University, Strasbourg, France; the University of Siegen, Siegen, Germany; University of Innsbruck, Innsbruck, Austria; University of Alcala, Alcala de Henares, Spain; University Tor Vergata, Rome, Italy; the Universidad Pontificia de Salamanca, Madrid, Spain; University of Camerino, Camerino, Italy; and the Swiss Center for Scientific Computing, Manno, Switzerland. Since 1981, he has been a Professor with the Department of Applied Electronics and Information Engineering, Faculty of Electronics, Telecommunications and Information Technology, UPB. Since 1993, he has been a Scientist with the German Aerospace Center (DLR), Wessling, Germany. He is developing algorithms for model-based information retrieval from high-complexity signals and methods for scene understanding from very-high-resolution synthetic aperture radar (SAR) and interferometric SAR data. Since 2011, he has been leading the Immersive Visual Information Mining Research Laboratory, Munich Aerospace Faculty, and he is the Director of the Research Center for Spatial Information, UPB. Since 2001, he had been initiating and leading the Competence Center on Information Extraction and Image Understanding for Earth Observation, ParisTech, Paris Institute of Technology, Telecom Paris, Paris, France, a collaboration of DLR with the French Space Agency (CNES). He has been a Professor with the DLR-CNES Chair, ParisTech, Paris Institute of Technology, Telecom Paris. He has initiated the European frame of projects for image information mining (IIM) and is involved in research programs for information extraction, data mining and knowledge discovery, and data understanding with the European Space Agency (ESA), NASA, and in a variety of national and European projects. He and his team have developed and are developing the operational IIM processor in the Payload Ground Segment systems for the German missions, TerraSAR-X, TanDEM-X, and the ESA Sentinel-1 and Sentinel-2. He is a Senior Scientist and the Data Intelligence and Knowledge Discovery Research Group Leader with the Remote Sensing Technology Institute, DLR. His research interests include explainable and physics aware Artificial Intelligence, smart sensors design, and qauntum machine learning with applications in Earth Observation.

Dr. Datcu is a member of the ESA Working Group Big Data from Space. He was the recipient of the Best Paper Award and the IEEE Geoscience and Remote Sensing Society Prize, in 2006, the National Order of Merit with the rank of Knight, for outstanding international research results, awarded by the President of Romania, in 2008, and the Romanian Academy Prize Traian Vuia for the development of the SAADI image analysis system and his activity in image processing, in 1987. He was also the recipient of the Chaire d'excellence internationale Blaise Pascal 2017 for international recognition in the field of data science in earth observation. He has served as a Co-organizer for international conferences and workshops and as Guest Editor for a special issue on AI and Big Data of the IEEE and other journals.